RARE METALS
Vol. 29, No. 3, Jun 2010, p. 292
DOI: 10.1007/s12598-010-0051-1

Directional solidification of Ti-45Al-8Nb-(W,B,Y) alloy

DING Xianfei, LIN Junpin, HE Jianping, YE Feng, and CHEN Guoliang

State Key Laboratory for Advanced Metals and Materials, University of Science and Technology Beijing, Beijing 100083, China

Received 16 May 2009; received in revised form 9 July 2009; accepted 12 August 2009

Abstract

Using a Bridgman vertical vacuum furnace, Ti-45Al-8Nb-(W,B,Y) (at.%) bars, which were prepared from a plasma arc melting (PAM) ingot, were directionally solidified at growth rates of 10, 15, and 20 μm/s. Polysynthetic twinned (PST) crystal with an aligned lamellar microstructure was obtained at the growth rate of 15 μm/s because of high Nb addition. The principle of PST crystal growth and the effect of Nb element were discussed. The results of investigations on microstructure and micromechanical properties of the directionally solidified (DS) bars of Ti-45Al-8Nb-(W,B,Y) alloy are briefly summarized.

Keywords: directional solidification; TiAl alloys; lamellar microstructure; crystal growth

1. Introduction

High Nb containing TiAl alloys have better tensile strength, oxidation resistance, and creep properties at elevated temperature compared with conventional TiAl alloys [1-3]. Nb has become a critically important alloying element in gamma titanium aluminide alloys. High Nb addition can significantly improve the high-temperature properties of TiAl-based alloys.

The fully lamellar structure of TiAl(γ)/$Ti_3Al(\alpha_2)$ two-phase alloy is considered as the most favorable for forthcoming applications, owing to its superior fracture toughness and creep resistance as compared those of any other microstructure types [4-5]. Lamellar orientation, one of the major microstructural variables influencing the mechanical properties of TiAl, can be controlled by the directional solidification (DS) technique. In this respect, polysynthetic twinned (PST) crystals of TiAl-based alloys had been extensively studied [6-9].

There are two ways to achieve PST TiAl alloys: one is the seeding technique and the other is modifying the solidification process without using the seeding technique [10]. PST crystal growth with high Nb containing TiAl alloy is different from that with other TiAl-based alloys reported by Johnson [11], Lee [12], Kim [13], and so on. Most of them achieved preferred lamellar orientation by controlling the primary solidification α-(Ti) phase or by means of a seeding technique. However, it had not been reported that PST crystal was achieved by modifying the solidification process and the composition of a TiAl alloy without using a seed technique.

In this paper, DS Ti-45Al-8Nb-(W,B,Y) alloy with an aligned lamellar microstructure was obtained by using a Bridgeman vertical vacuum furnace. The purpose of this paper is to try to explain why the β-(Ti) primary solidified phase of high Nb containing TiAl can form PST crystal in DS process, and the results of recent studies on the microstructures and the micromechanical properties of PST bars of high Nb containing TiAl alloys were briefly summarized.

2. Experimental

Ti-45Al-8Nb-(W,B,Y) alloy with the chemical composition of Ti-45.27Al-7.89Nb-(W,B,Y) (at.%) was prepared from a plasma arc melting (PAM) ingot. The ingot was cut into smaller bars using electro spark machining. Master bars (7 mm in diameter and 80 mm in length) were placed into an alumina crucible coated by yttria and heated to 1973 K with an induced graphite heater in order to achieve no magnetic interference of solidification under 380 Pa high-purity argon. After heating-up and holding for 30 min, the samples were pulled downward. Three bars were grown at a constant temperature gradient of $G_L = 15 \times 10^3$ K/m and growth rates of 10, 15, and 20 μm/s, respectively. At the end of the pulling, quenching was operated immediately.

The DS bars were sectioned longitudinally and trans-

Corresponding author: DING Xianfei **E-mail:** xianfeimail@gmail.com

versely and were polished and etched in a solution of 5 mL HF, 10 mL HNO_3, and 85 mL H_2O. An optical microscope (OM) was used to characterize the optical microstructure. Microstructure analyses were conducted with the use of field emission scanning electron microscope (FEM), employing the back-scattered electron (BSE) imaging. The lamellar fracture structures were characterized by scanning electron microscopy (SEM). Compositions of the various microstructural constituents were determined by electron probe micro-analyzer (EPMA). Microhardness measurements were performed with a nanoindenter at a strain rate of 0.05 s^{-1} on the longitudinal sections of DS bars.

3. Results and discussion

3.1. Microstructure of DS Ti-45Al-8Nb-(W,B,Y) bars

3.1.1. Optical microstructure

Fig. 1 shows the longitudinal OM images of DS bars at constant growth rates of 10, 15, and 20 μm/s. The growth beginning interface sections and the quenching sections of the bars were all represented. Other sections in the DS region had similar appearances just like that of the growth beginning. Only at the growth rate of 15 μm/s, PST crystal with the aligned lamellar boundaries was observed. DS bars at growth rates of 10 and 20 μm/s were fully occupied by blocks of unaligned lamellar microstructures, which consisted of crystal grains with different sizes, and the lamellar orientations inside the grains inclined at angles of 0°, 45°, and 90° to the growth direction. Therefore, the DS bar at 15 μm/s had been studied specially in this paper. As an unfortunate result of the crucible set a little inclination to the central axis, PST crystal was grown at an angle to the bar axis, which can be seen clearly from the quenching interface.

3.1.2. Electron microstructure

Fig. 2 shows the BSE micrograph near the quenching interface of the DS bar at a growth rate of 15 μm/s. The secondary arms oriented at 90° to the primary dendrite spines should be cubic β phase, whereas those inclined at an angle of 60° should be hcp α phase. At the solid/liquid interface, both angular dimensions were observed at the front of the solidified reaction. Other included angles were not exactly equal to above-mentioned angle sizes, because the specimen was not cut exactly along the primary dendrite spines. In fact, primary β phase and α phase that all formed from the liquid was reported in ternary Ti-Al-M systems when M is a β-stabilizing element, such as Nb [14]. At a given growth rate, both β and α phase could be primary solidified phase in DS process.

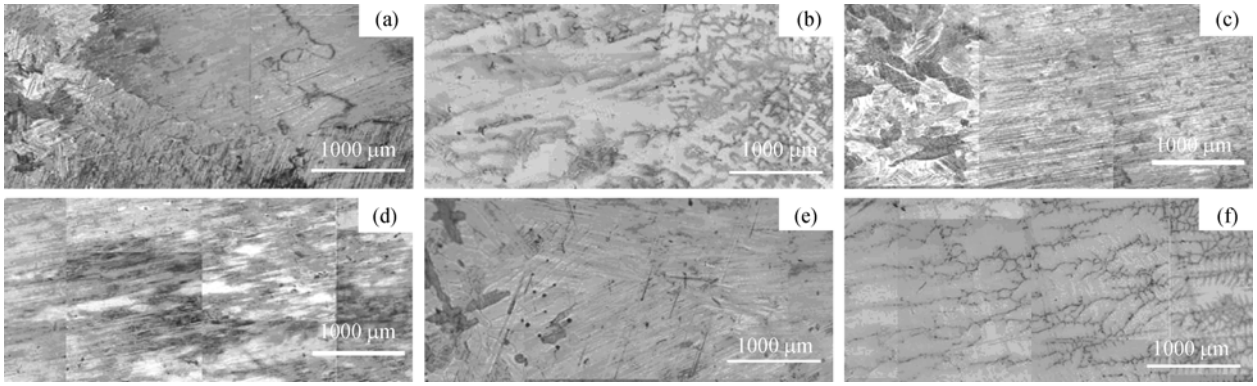

Fig. 1. Longitudinal microstructures from growth beginning and quenching sections of the DS bars at different growth rates: (a) section of growth beginning at 10 μm/s; (b) section of quenching at 10 μm/s; (c) section of growth beginning at 15 μm/s; (d) section of quenching at 15 μm/s; (e) section of growth beginning at 20 μm/s; (f) section of quenching at 20 μm/s.

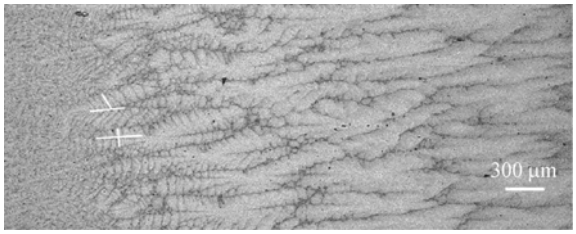

Fig. 2. BSE image of quenched solid-liquid interface in the DS bar at a growth rate of 15 μm/s.

β phase formed from the liquid phase makes the lamellar boundary inclined at an angle of 0° or 45° to the growth direction, and α phase formed leads to the lamellar boundary perpendicular to the growth direction [14]. Therefore, the aligned lamellar boundary paralleling to the growth direction means that α phase was abnormally formed from liquid. As represented later in this paper, Ti-45Al-8Nb-(W,B,Y) corresponds to Ti-46.5Al in binary composition. With the aid of the binary phase diagram, we can presume that aligned lamellar orientation should be realized with three stages. Fig. 3 and Fig. 4 schematically illustrate a vertical section of the partially melted grown crystal and corre-

sponding position in the binary phase diagram during DS process.

For stage one, when primary β cellular dendrites with a lower Al content and a higher solidified temperature are first formed in the melted alloy, a large quantity of Al is rejected to the interdendritic region (Fig. 3(a)), where the corresponding constituent slightly shifts to the Al-rich side of the phase diagram, and it can be at the content extent of primary α solidified. As shown in Fig. 4, A_0 is the mean composition of the master bar, A_1 is the initial composition of primary β dendrite, and A_2 is the composition of β interdendrite. Fortunately, Nb addition has greatly increased the temperature of initiative β → α transformation. For stage two, with the temperature gradient away from the interface partial melting, primary β transforms to α phase through the β → α transformation, while β interdendritic area still keeps melting as the result of $T_2 < T_1$ (Fig. 3(b) and Fig. 4). The orientational relationship between α and β phases is $(110)_\beta$ // $(0001)_\alpha$ [15]. When the temperature decreases more in the last stage, primary α phase also precipitates from the β interdendritic liquid (Fig. 3(c)). The most important in this stage is that the primary α phase can grow on the top of the previous solid-state transformed α phase and keeps the orientation relationship with it. At last, aligned lamellar structure is formed in α phase with Blackburn's orientation relationship

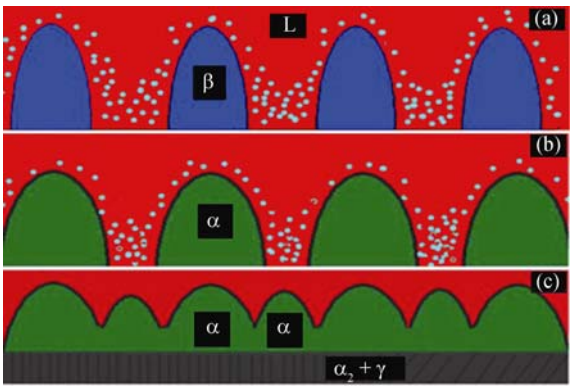

Fig. 3. Schematic DS procedure with Ti-45Al-8Nb-(W,B,Y) alloy.

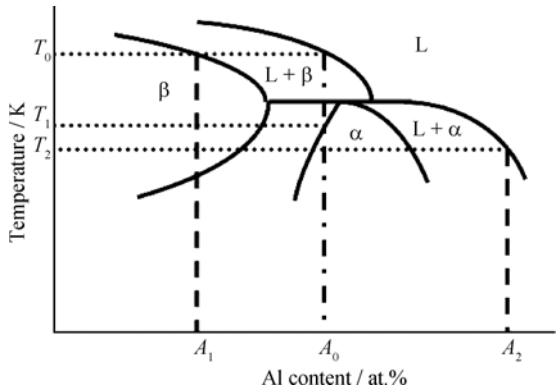

Fig. 4. Schematic Ti-Al binary phase diagram.

of $(0001)_\alpha$ // $(111)_\gamma$, $<11\bar{2}0>_\alpha$ // $<1\bar{1}0>_\gamma$ [16].

In fact, the lamellar boundary aligned in this manner deeply depends on growth rate (R) and cooling rate. The growth rate of primary β phase is related to the composition of β interdendritic region and also related to the condition of primary α phase growth, while the cooling rate associates with the composition. The content of Al in primary β interdendrite in the high-speed quenching region in Fig. 5(d) detected by EPMA even can reach 74.62 at.%. With the growth of β, interdendritic Al continuously diffuses to primary solidified β so that α phase also precipitates in interdendrite. Aligned lamellar microstructure was achieved under the condition that G_L/R rate should be in an appropriate range. Faster growth rate with less Al diffusion induces too more density of Al in β interdendrite to growth of α phase, and a lower growth rate accompanied by a lower Al in β interdendrite cannot align the orientation of primary α phase with the orientation of the solid-state transformed α, or even cannot form primary α. Out of the range, the PST crystal will never be achieved successfully.

Fig. 5 shows the typical microstructures from the DS beginning to the quenching region. Some Y_2O_3 and Al_2O_3 particles were detected in the high-temperature section of the bar. These particles come from the coating and crucible. They will not change the lamellar orientation but largely decrease the mechanical properties of the DS bar. In order to eliminate these ceramic inclusions, a better crucible that does not react with titanium at high temperature should be studied and applied next. As seen in Fig. 5(a), it can be clearly identified that B2 segregation that inevitably exists in as-cast microstructure with reticular morphology disappears in the DS region. Some Y_2O_3 particles appear in hexapetalous snow blossoms, and few precipitate phases that are rich in Ti, Nb, and W cross over the laminar structure, as shown in Figs. 5(b) and 5(c). The chemical composition of the ceramic particles was determined by EPMA to be (39.12 ± 0.87) at.% of Y and (60.88 ± 1.03) at.% of O. The composition of (Ti,Nb,W) precipitate phases is shown in Table 1. At the regions of directional solidification and quenching, inclusion particles and precipitate phases almost centralize in primary β dendritic boundaries with Al-rich zones (Figs. 5(d), 5(e), and 5(f)). Cellular morphology is observed in the DS region, and the lamellar orientation is not changed in the cell boundaries and segregation region.

When the primary β phase grows, Al and inclusion particles, such as Y_2O_3 and Al_2O_3, are consequently rejected to the interdendritic region (Figs. 5(d), 5(e), and 5(f)). β phase contains lower Al content and higher β-formers additions such as Nb and W. As a result, the interdendritic area exhibits black contrast because it is rich in Al and poor in Nb and

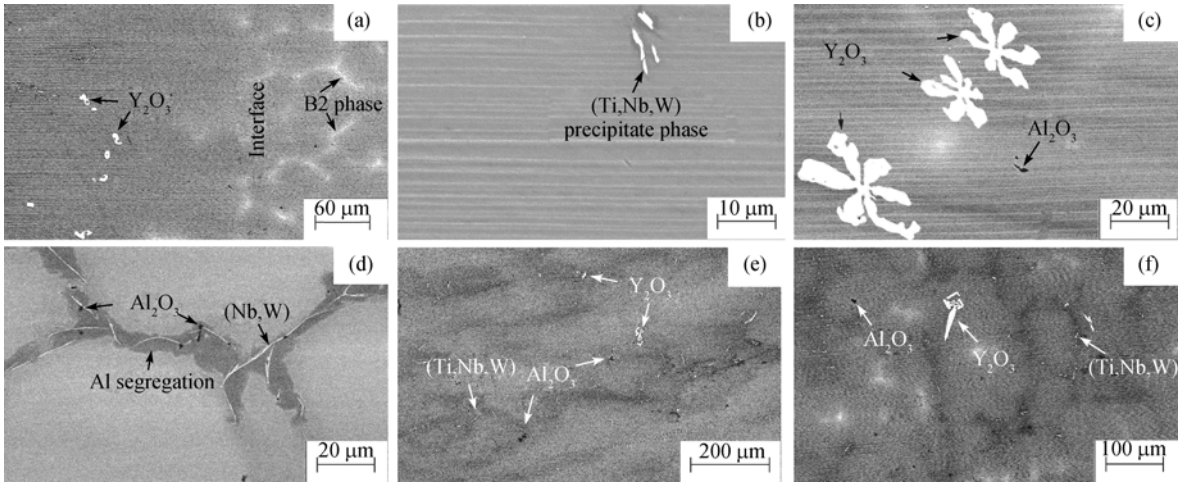

Fig. 5. BSE microstructures of the DS Ti-45Al-8Nb-(W,B,Y) alloy at a growth rate of 15 μm/s: (a) growth beginning interface; (b) (Ti,Nb,W) precipitate phase; (c) morphology of Y_2O_3 and Al_2O_3 particles; (d) quenched interdendrite; (e) cellular morphology in the longitudinal section; (f) cellular morphology in the transversal section.

Table 1. Chemical composition of the (Ti,Nb,W) precipitate phase at.%

Ti	Nb	W	Al
66.99 ± 0.42	24.07 ± 0.24	2.07 ± 0.29	6.86 ± 0.28

W. As the temperature falls down, the β → α transformation should take place, and the β interdendritic primary α phase also come into being. Al element will diffuse to previous solid-state transformed α phase, while the β-formation elements, such as Nb and W, will go in the opposite direction. This tendency leads to enriching in Nb and W and depletion in Al at the interface between previous solid-state transformed α phase and primary α phase. Because the cooling rate is fast, Nb and W have small chance to diffuse and to be enriched. Finally, some precipitate phases, which are rich in Ti, Nb, and W, in place large-area of B2 segregation, cross over the laminar structure.

3.2. Microstructure of fracture

To see the lamellar structure more clearly in three dimensions, we broke the PST crystal with one stroke in the direction of normal to lamellar boundary. It was found that the fracture plane is inclined with an angle of about 45° to lamellar boundary, which agrees to the dependence of the strength with the angle between the lamella boundary and the loading axis; in what follows, the direction of inclination about 45° to lamellar boundary is the weakest direction on the PST-TiAl crystal [15].

Fig. 6 shows the micrographs of fracture in the direction of the normal to fracture plane. An overwhelming number of lamellar structure consists of homogeneous γ/α_2 lamina with a thickness of 1-2 μm. With the exception of it, fractional lamella with thickness that can reach up to 4-5 μm makes up the lamina-like microstructure (Fig. 6(b)). The uneven lamellar microstructures, which can also be seen in Figs. 5(c) and 5(d), may affect the deformation consistency in themselves.

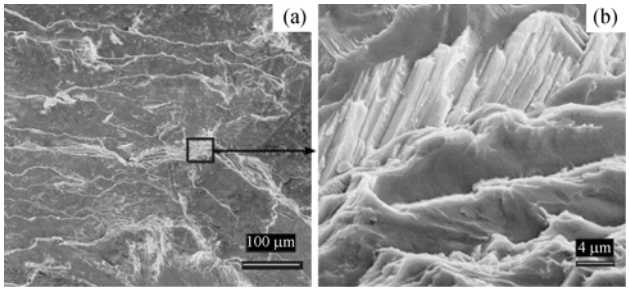

Fig. 6. Fractographs of the DS Ti-45Al-8Nb-(W,B,Y) alloy at a growth rate of 15 μm/s: (a) at low magnification; (b) at high magnification.

3.3. Micromechanical properties

Since tensile properties became meaningless because Y_2O_3 and Al_2O_3 particles came into the PST crystal of Ti-45Al-8Nb-(W,B,Y) alloy, the microhardness was measured to predict the mechanical properties of the PST. Each measurement was performed in only lamellar structure without Y_2O_3 and Al_2O_3 particles. As shown in Fig. 7, the area surrounding the growth beginning interface was chosen and the microhardness in three regions was measured: as-cast region, transition region, and DS region. It was found that a well-aligned lamellar microstructure can obviously decrease the microhardness and yield stress.

3.4. Effect of Nb element

Nb is reported to be one of the most important elements for providing TiAl-based alloys with good oxidation resistance and high-temperature mechanical properties. Nb is

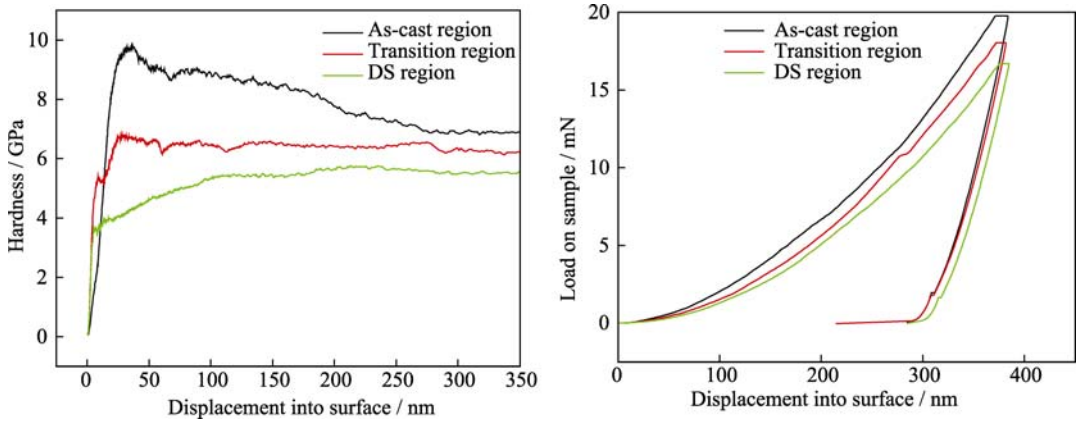

Fig. 7. Micromechanical properties in different regions of the DS bar at the growth rate of 15 μm/s: (a) hardness-displacement curve; (b) load-displacement curve.

β-formation element that can shift the TiAl binary phase boundaries to the Al-rich side. According to Kim [13] and Kim [17], Ti-45Al-8Nb-(W,B,Y) alloy shifts the compositions corresponding to binary alloy that is approximately Ti-46.5Al, wherein its primary solidified phase is β. It can also be identified by noting that the dendrite arms are orthogonal to one another on the BSE image of as-cast Ti-45Al-8Nb-(W,B,Y) alloy (Fig. 8).

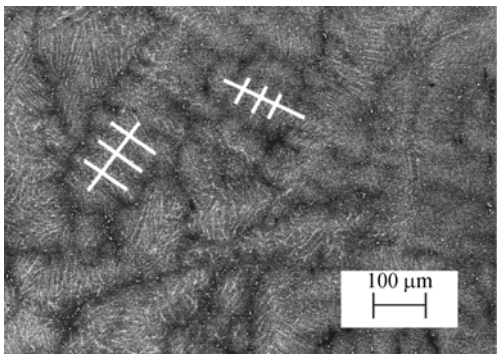

Fig. 8. BSE image of as-cast Ti-45Al-8Nb-(W,B,Y) alloy after arc-melting.

By high Nb addition, the temperature of β → α transformation increases so greatly that it exceeds the temperature of primary α phase formed in the β interdendritic area, which gives the possibility to form aligned α phase at high temperature. The phase boundary changed by Nb addition is shown in the 8Nb-TiAl quasi-phase diagram (Fig. 9) by Chen [1]. On the other hand, the addition of Nb makes the α → γ transformation kinetics sluggish [18] which is advantageous in getting more time to grow α phase in all of interdendritic regions and aligning all of α phase at high temperature. Moreover, no segregation of Nb would take place at the interfaces in the lamellar microstructure formed along the pathway because niobium is partitioned to α and γ phases equally. That also indicates that the relative thermal stability among the interfaces remains unchanged with and without niobium. All of these assist that the PST of primary β TiAl alloy with high Nb addition is realized without using a seeding technique.

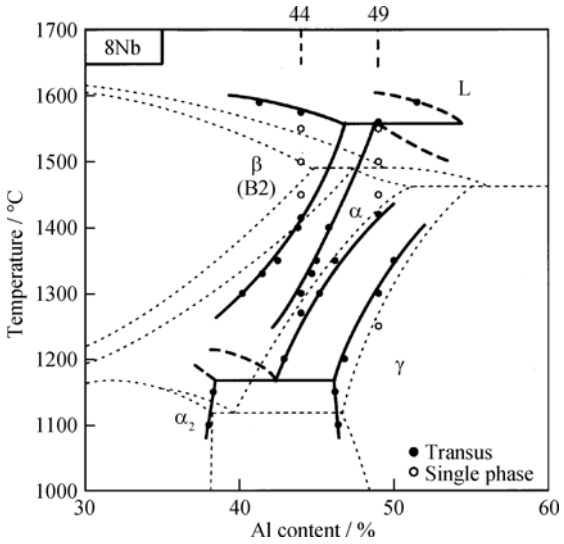

Fig. 9. 8Nb-TiAl quasi-phase diagram [1].

4. Conclusions

(1) PST Ti-45Al-8Nb-(W,B,Y) crystal was achieved without using a seeding technique at the growth rate of about 15 μm/s even though β was the primary solidification phase for this alloy. During growth, primary α phase precipitated from the β interdendritic liquid, grew on the previous solid-state transformed α phase, and eventually kept the orientation relationship with it.

(2) B2 segregation, which generated inevitably in as-cast microstructure, disappeared in the DS region. Y_2O_3 and Al_2O_3 particles that came from the crucible and coating were centralized around the boundary of primary β dendrite.

(3) PST crystal obviously decreased the microhardness and yield stress of Ti-45Al-8Nb-(W,B,Y) alloy at room temperature.

Acknowledgement

This research was financially supported by the National Natural Science Foundation of China (No. 50771013).

References

[1] Chen G.L., Zhang W.J., Liu Z.C., Li S.J., and Kim Y.W., Microstructure and properties of high-Nb containing TiAl-base alloys, [in] *Proceedings of Symposium held during the 1999 TMS Annual Meeting*, San Diego, 1999: 371.

[2] Xu X.J., Lin J.P., Wang Y.L., Gao J.F., Lin Z., and Chen G.L., Microstructure and tensile properties of as-cast Ti-45Al-(8-9)Nb-(W, B, Y) alloy, *J. Alloys Compd.*, 2006, **414** (1-2): 131.

[3] Lin J.P., Xu X.J., Wang Y.L., He, S.F, Zhang, Y., Song, X.P., and Chen, G.L., High temperature deformation behaviors of a high Nb containing TiAl alloy, *Intermetallics*, 2007, **15** (5-6): 668.

[4] Yamaguchi M. and Inui H., TiAl compounds for structural applications, [in] *Proceedings of the First International Symposium on Structural Intermetallics*, Warrendale, 1993: 127.

[5] Kim Y.W. and Boyer R.R., Microstructure/property relationships in titanium aluminides and alloys, [in] *Proceedings of the Symposium on Microstructure/Property Relationships in Titanium Aluminides and Alloys Presented at the 1990 TMS Fall Meeting*, Detroit, 1990: 674.

[6] Johnson D.R, Masuda Y., Inui H., and Yamaguchi M., Alignment of the TiAl/Ti_3Al lamellar microstructure in TiAl alloys by growth from a seed material, *Acta Mater.*, 1997, **45** (6): 2523.

[7] Liu Y., Wang D., Chen D., Lin D.L., Chen S.P., and Liu Z.G., Microtwinning deformation in PST TiAl crystal, *Acta Metall. Sin.*, 1995, **9** (31): 393.

[8] Su J.L. and Hu G.K., Micromechanical model for γ-TiAl base PST crystals, *Acta Metall. Sin. Eng. Lett.*, 2005, **18** (6): 686.

[9] Asai T., Hirata S., Takeyama M., and Matsuo T., Microstructure in Ti-48at.%Al PST crystal subjected to creep deformation, *Mater. Sci. Eng. A*, 2002, **329-331**: 828.

[10] Jung I.S., Jang H.S., Oh M.H., Lee J.H., and Wee D.M., Microstructure control of TiAl alloys containing β stabilizers by directional solidification, *Mater. Sci. Eng. A*, 2002, **329-331**: 13.

[11] Johnson D.R., Inui H., Muto S., Omiya Y., and Yamanaka T., Microstructural development during directional solidification of α-seeded TiAl alloys, *Acta Mater.*, 2006, **54** (4): 1077.

[12] Lee H.N., Johnson D.R., Inui H., Oh, M.H., Wee D.M., and Yamaguchi M., Microstructural control through seeding and directional solidification of TiAl alloys containing Mo and C, *Acta Mater.*, 2000, **48** (12): 3221.

[13] Kim J.H., Kim S.W., Lee H.N., Oh M.H., Inui H., and Wee D.M., Effects of Si and C additions on the thermal stability of directionally solidified TiAl-Nb alloys, *Intermetallics*, 2005, **13** (10): 1038.

[14] Kim M.C., Oh M.H., Lee J.H., Inui H., Yamaguchi M., and Wee D.M., Composition and growth rate effects in directionally solidified TiAl alloys, *Mater. Sci. Eng. A*, 1997, **239-240**: 570.

[15] Johnson D.R., Masuda Y., Shimada Y., Inui H., and Yamaguchi, M., Directional solidification of TiAl-based alloys, [in] *Proceedings of 2nd International Symposium on Structural Intermetallics*, Champion, 1996: 287.

[16] Blackburn M., *Science, Technology and Application of Titanium*, Edtited by Jaffee R.T. and Promisel N.E., Pergmon Press, London, 1970: 633.

[17] Kim S.W., Wang P., Oh M.H., Wee D.M., and Kumar K.S., Mechanical properties of Si- and C-doped directionally solidified TiAl-Nb alloys, *Intermetallics*, 2004, **12** (5): 499.

[18] Takeyama M., Ohmura Y., Kikuchi M., and Matsuo T., Phase equilibria and microstructural control of gamma TiAl based alloys, *Intermetallics*, 1998, **6** (7-8): 643.